Polish Journal of Veterinary Sciences Vol. 26, No. 3 (2023), 367–376

DOI 10.24425/pjvs.2023.145042

Original article

Andrographolide loaded montmorillonite attenuated enterotoxigenic *Escherichia coli* induced intestinal barrier injury and inflammation in a mouse model

P. Wang, L. Li, L. Gan, Q. Chen, H. Qiao, W. Gao, Y. Zhang, J. Wang

College of Biology Engineering, Henan University of Technology, Zhengzhou, China

Abstract

Montmorillonite (MMT), a natural absorbent agent, has widely been accepted for its anti-diarrhea function in human and farm animals; however, its specific physicochemical property limits its biological function in practical use. In the current study, raw MMT was loaded by andrographolide, namely andrographolide loaded montmorillonite (AGP-MMT). The microstructure of AGP-MMT was observed by scanning electron microscope (SEM) and X-ray diffraction (XRD). The effect of AGP-MMT on the growth performance, intestinal barrier and inflammation was investigated in an enterotoxigenic *Escherichia coli* (ETEC) challenged mice model. The results show that the microstructure of MMT was obviously changed after andrographolide modification: AGP-MMT exhibited a large number of spheroid particles, and floccule aggregates, but lower interplanar spacing compared with MMT. ETEC infection induced body weight losses and intestinal barrier function injury, as indicated by a lower villus height and ratio of villus height/crypt depth, whereas the serum levels of diamine oxidase (DAO), D-xylose and ETEC shedding were higher in the ETEC group compared with the CON group. Mice pretreated with AGP-MMT showed alleviated body weight losses and the intestinal barrier function injury induced by ETEC challenge. The villus height and the ratio of villus height/crypt depth, were higher in mice pretreated with AGP-MMT than those pretreated with equal levels of MMT. Pretreatment with AGP-MMT also alleviated the increased concentration of serum tumor necrosis factor-α (TNF-α) and interleukin-1β (IL-1β), and the corresponding genes in the jejunum induced by ETEC infection in mice. The protein and mRNA levels of IL-1β were lower in mice pretreated with AGP-MMT than those with equal levels of MMT. The results indicate that AGP-MMT was more effective in alleviating intestinal barrier injury and inflammation in mice with ETEC challenge than MMT.

Keywords: montmorillonite, andrographolide modified montmorillonite, enterotoxigenic *Escherichia coli*, intestinal barrier, inflammation

Correspondence to: J. Wang, e-mail: wangjr@haut.edu.cn

Introduction

Enterotoxigenic *Escherichia coli* (ETEC) is one of the most common bacterial causes of morbidity and mortality in children and farm animals (Gaastra and Svennerholm 1996, Ma et al. 2021). The most typical manifestation of ETEC infection is diarrhea. ETEC infection leads to acute watery diarrhea and subsequent intestinal barrier injury and inflammation (Sargeant et al. 2010, Brubaker et al. 2021). It is expected that ETEC stress may be alleviated by maintaining the intestinal barrier function, thus protecting intestinal health. Antibiotics are the most popular treatment, but the occurrence of antibiotic resistance genes, which transfer to human pathogens, and the clearance of beneficial intestinal microorganisms (Bywater 2005, Rodas et al. 2011) prompted us to find alternative treatments to deal with ETEC infection.

Montmorillonite (MMT), also known as dioctahedral montmorillonite, is a natural alumino-magnesium silicate with multiple physicochemical properties, such as absorption and ion exchange capacity. MMT has been widely accepted as an anti-diarrhea agent in many countries for its safety and ease of access, though it is not recommended as the first-line medicine (Guarino et al. 2009, Hu et al. 2012, Guarino et al. 2014, Chen et al. 2018). In addition, MTT also exhibits a beneficial effect on the growth performance and intestinal health of farm animals (Liu et al. 2020). Growing evidence has implicated MMT as a natural mineral and drug carrier (Massaro et al. 2018, Liu et al. 2020), and modified MMT with a mineral, such as copper, exhibited an enhanced growth promoting role in broilers by regulating intestinal barriers, the anti-inflammatory response, and anti-oxidant capacity (Wang et al. 2022). Plant extracts has attracted widespread attention for its safety and effectiveness against certain pathogenic bacteria (Cheng et al. 2014, Vaseeharan and Thaya 2014). Andrographolide is the main active component of the medicinal plant Andrographis paniculate, which has been widely used in China and Southeast Asia (Abu-Ghefreh et al. 2009), and possesses diverse biological functions, including anti-inflammatory and antioxidant (Burgos et al. 2021). However, the low aqueous solubility, poor bioavailability, and short half-life of andrographolide limits its biological activity (Ghosh et al. 2016). These disadvantages can be mitigated by the use of a suitable delivery system. Therefore, andrographolide loaded MTT is a promising strategy for enhancing its function in response to ETEC infection.

The purpose of this study was to investigate the loading capacity of MMT for andrographolide intercalation and its protection function on the intestinal health of mice with ETEC infection.

Materials and Methods

Materials

The raw MMT used in this study was produced in Mongolia, China. Andrographolide was purchased from the Shanghai Tongtian biotech company with a purification above 98 percent.

Preparation of andrographolide modified montmorillonite (AGP-MMT) and analysis

The AGP-MMT was prepared after sodium modification, polyethylene glycol modification and andrographolide modification of the raw MMT. Briefly, the raw MMT was mixed with water in a mass ratio of 1:8, about 4.0% sodium carbonate was further added and stirred for 2 h to achieve a homogenized slurry. About 10 g of sodium modified MMT was mixed with 0.4 g polyethylene glycol and mixed for 1.5 h at 60°C. Finally, the polyethylene glycol modified MMT was mixed with andrographolide at a ratio of 5:1, the AGP-MMT was acquired after mixing, drying and grinding through a 200 mesh sieve.

The andrographolide concentration in AGP-MMT was measured by high-performance liquid chromatography (SHIMADZU LC-10AT, Shimadzu, Japan). Andrographolide was separated on an Agilent TC-C18 analytical column (4.6 × 150 mm) at 25°C, the mobile phase was methanol with water. The flow rate was 0.8 mL/min, the injection volume was 10 μL and the detection wavelength absorbance was 225 nm. The concentration of andrographolide in AGP-MMT was calculated according to the standard curve between peak area and andrographolide content.

Structure analysis

Scanning electron microscope

The surface and microstructure of MMT and AGP-MMT samples were observed under a scanning electron microscope (SEM, Quanta 250FEG) at 20 kV and 80 μA.

X-ray diffraction

MMT and AGP-MMT samples were examined by XRD using Cu-Kα radiation (λ=1.5406 nm) under 40 kV and 30 mA. Samples were continuously scanned from 0° to 85° at 5°/min. The intercalated structures were identified using Bragg's relation: $\lambda=2d\sin\theta$, where, 'λ' is the wavelength of X-ray, 'd' is the interplanar spacing in a crystalline sample and 'θ' is the angle of the diffraction.

Animals and experiment

All experiments performed were approved by the Animal Care and Use Committee of Henan University of Technology (Ethic Approval Code: Hena202105-1), and were performed in accordance with the National Research Council's Guide for the Care and Use of Laboratory Animals, Chinese Order No.676 of the State Council, 1 March 2017.

A total of forty-eight male Kunming mice with a similar age and body weight were randomly assigned to control group (CON), ETEC group (ETEC), low levels of AGP-MMT(AGP-MMT-L), medium levels of AGP-MMT(AGP-MMT-M), high levels of AGP-MMT (AGP-MMT-H), and high levels of MMT (MMT-H), with eight repeats per group. After one week adaption, ETEC, AGP-MMT-L, AGP-MMT-M, AGP-MMT-H, and MMT-H were challenged with ETEC on day 8 as previously described (Ren et al. 2014). From day 9 to 15, AGP-MMT-L, AGP-MMT-M and AGP-MMT-H group mice were orally gavaged with 0.4, 0.8 and 1.2 g/kg, respectively. Mice in the MMT-H group were orally gavaged with the same amount of MMT as AGP-MMT-H, and mice in the CON group were orally gavaged with saline. All mice were sampled at day 16 after 12 h fasting.

ETEC counting

ETEC in feces was measured as previously described (Wang et al. 2022). Briefly, the fresh feces were collected and homogenized in saline and plated on MacConkey agar through gradient dilution. After 24 h incubation at 37°C, Colony-forming unite (CFU) were counted. The concentration of *Escherichia coli* was expressed by the log CFU per gram of feces or tissues.

Real-time RT-PCR

All primers were designed through primer BLAST from NCBI as previously described (Wang et al. 2022). Total RNA of frozen samples was extracted using the RNAiso Plus reagent, and the complementary DNA (cDNA) was synthesized using a reverse transcription kit. Real-time quantitative PCR (RT-qPCR) was performed on a CFX96 Real-Time PCR Detection System (Analytik Jena, Jena, Germany) to quantify mRNA expression with a commercial SYBR Green kit. β-actin was used as the internal control. The gene expression levels of different samples were compared using the $2^{-\Delta\Delta CT}$ method.

Intestinal morphology analysis

The middle part of the jejunum tissue was fixed in paraformaldehyde, dehydrated and embedded in paraffin wax. The tissue slices of jejunum were further stained with hematoxylin. Villus height, crypt depth and villus height/crypt depth were determined.

Inflammatory cytokine analysis

The serum TNF-α and IL-1β were measured using a mouse-specific ELISA kit (Nanjing Jian Cheng Co., Ltd., Nanjing, China) according to the standard procedures of the protocol. The concentrations of serum TNF-α and IL-1β were calculated according to the standard curve, which was drawn by ELISACalc software V0.1.

Intestinal permeability analysis

Intestinal permeability was assessed by determining the serum levels of DAO and D-xylose. DAO and D-xylose were measured using a mouse-specific kit (Nanjing Jiancheng Bioengineering Co., Ltd., China) according to the standard procedures of the protocol.

Data analysis

All data are expressed as means ± sem. The one-way ANOVA procedure of SAS 9.1.3 was used to analyze all data in this experiment, the Duncan method was used for multiple comparisons when the data normally distributed, while the NPAR1WAY procedure was used when the data were not normally distributed $p<0.05$ was considered as statistically significant.

Results

Microstructural characterization of AGP-MMT

The microstructural characterization of raw MMT and AGP-MMT was observed using SEM and XRD. The MMT mainly existed in the form of flake and aggregate, with the presence of larger particles and thicker flake. However, the AGP-MMT had a large number of spheroid particles in the gap between floccule aggregates, and the floccule aggregates increased and the outline was more prominent (Fig. 1A-B). The XRD results showed that the interplanar spacing was 1.546 and 1.336 nm in MMT and AGP-MMT, respectively (Fig. 1C-D), indicating the lower interplanar spacing in AGP-MMT compared with MMT. Andrographolide concentration in AGP-MMT was calculated according to the standard curve of andrographolide, and its concentration was 11.63%.

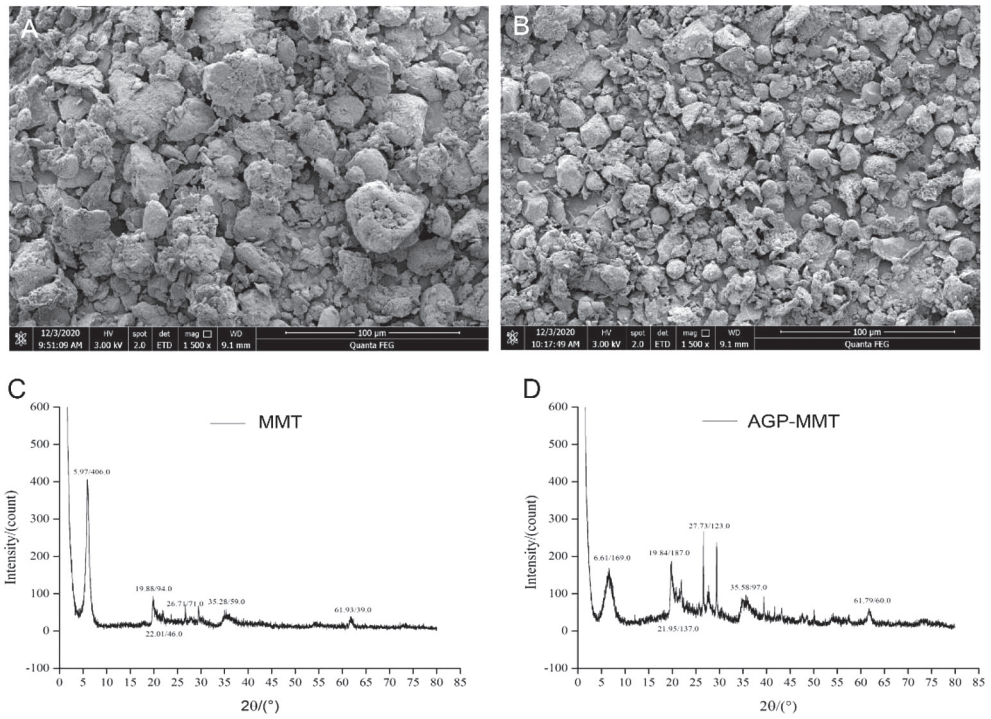

Fig. 1. Microstructure and X-ray diffraction of Montmorillonite (MMT) and andrographolide modified MMT (AGP-MMT). Microstructure of (A) MMT, (B) AGP-MMT observed by SEM (A and B x1500). X-ray diffraction diagrams of (C) MMT, and (D) AGP-MMT.

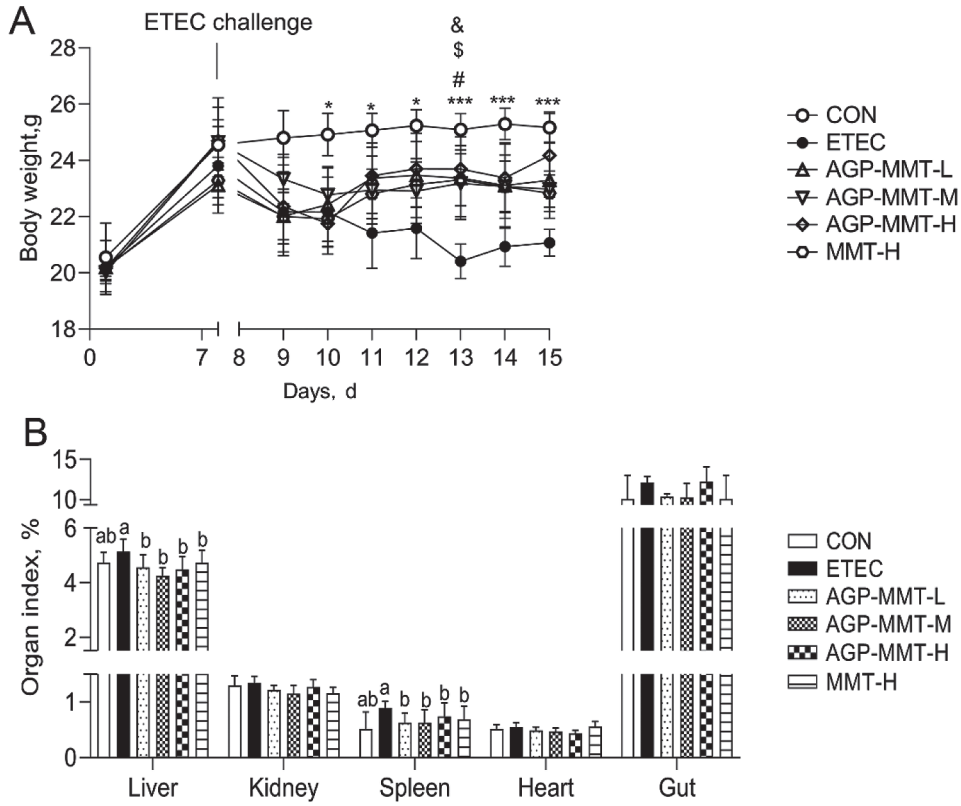

Fig. 2. Effect of different dose of AGP-MMT on body weight and organ index in ETEC challenged mice. Effect of different dose of AGP-MMT on (A) body weight, (B) organ index in mice with ETEC challenge. CON, control group; ETEC, enterotoxigenic Escherichia coli challenged group; AGP-MMT-L, ETEC+0.4 g/kg AGP-MMT; AGP-MMT-M, ETEC+0.8 g/kg; AGP-MMT-H, ETEC+1.2 g/kg AGP-MMT; MMT-H, equal amount of MMT with AGP-MMT-H. Data were expressed as means ± sem, n=8/group. *, **, *** represent $p<0.05$, $p<0.01$ and $p<0.001$ in the CON group compared with the ETEC group, respectively. #, $, & represent $p<0.05$ in the ETEC group compared with the AGP-MMT-M, AGP-MMT-H and MMT-H groups, respectively. Values within groups with different letters are significantly different ($p<0.05$).

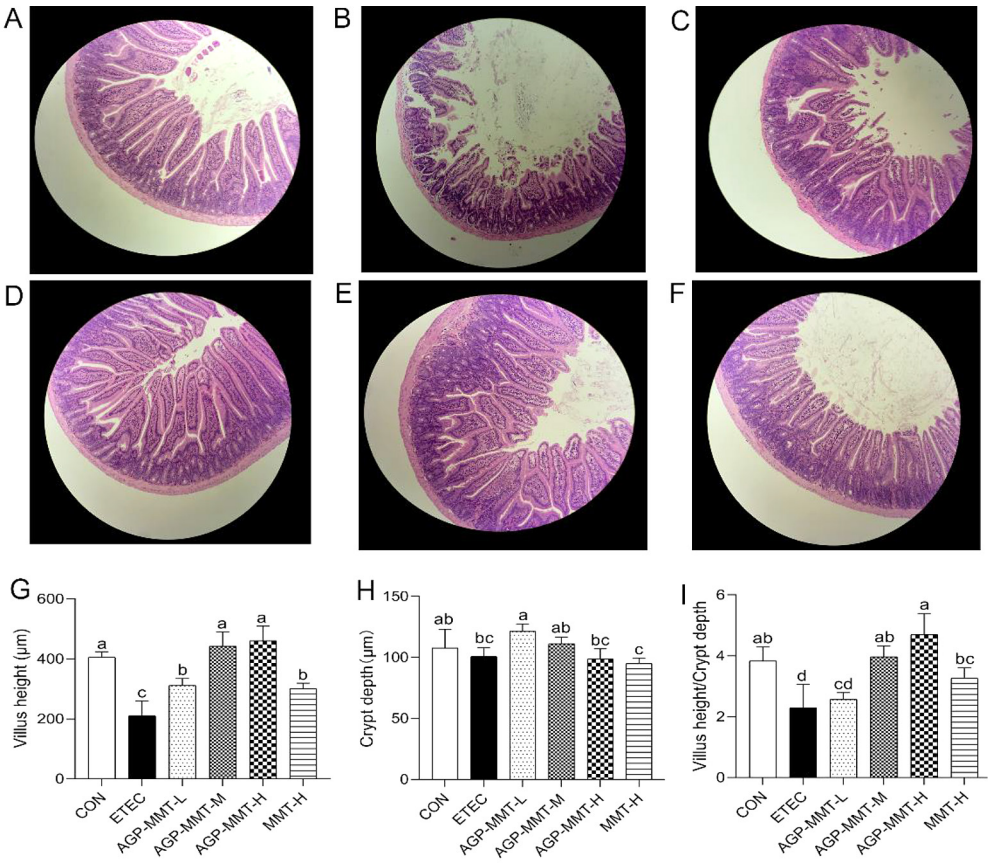

Fig. 3. Effect of different dose of AGP-MMT on the jejunum structure in ETEC challenged mice. The jejunum structure in the (A) control group (CON), (B) ETEC group (ETEC), (C) ETEC and low levels of AGP-MMT treated group (AGP-MMT-L), (D) ETEC and medium levels of AGP-MMT treated group (AGP-MMT-M), (E) ETEC and high levels of AGP-MMT treated group (AGP-MMT-H), (F) ETEC and high levels of MMT treated group (MMT-H). (G) villus height, (H) crypt depth, (I) villus height/crypt depth ratio of jejunum morphology in the CON, ETEC, AGP-MMT-L, AGP-MMT-M, AGP-MMT-H and MMT-H groups. Data were expressed as means ± sem, n=8/group. Values within groups with different letters are significantly different ($p<0.05$), Figs. A-F x100.

AGP-MMT alleviated body weight losses of mice with ETEC challenge

ETEC infection induced a great loss of body weight from day 8 till 15, compared with the CON group; however, the losses of body weight were significantly ($p<0.05$) alleviated in the groups of medium and high levels of AGP-MMT at day 13, whereas there was no significant effect ($p>0.05$) when low levels of AGP-MMT (AGP-MMT-L) treatment were given (Fig. 2A). Moreover, there was no significant difference ($p>0.05$) in body weight between AGP-MMT-H and MMT-H.

In line with the body weight, AGP-MMT-L, AGP-MMT-M, and MMT-H treatment significantly decreased ($p<0.05$) the hepatic and spleen index, compared with the ETEC group, and there was no significant difference ($p>0.05$) in hepatic and spleen index between the AGP-MMT-H and MMT-H group (Fig. 2B).

AGP-MMT alleviated intestinal injury in mice with ETEC challenge

ETEC treatment caused great histopathological damage (Fig. 3A-3B), The villus height and the ratio of villus height/crypt depth were significantly lower ($p<0.05$) in the ETEC group compared with the CON group. Mice pretreated with AGP-MMT significantly ($p<0.05$) attenuated the mucosal morphology damage in the jejunum of mice with ETEC infection (Fig. 3A-3E). Moreover, mice pretreated with AGP-MMT increased ($p<0.05$) the villus height and villus height/crypt depth, and decreased ($p<0.05$) crypt depth. In addition, the villus height and villus height/crypt depth were higher ($p<0.05$) in the AGP-MMT-H group compared with the MMT-H group (Fig. 3G-I), indicating a better alleviation role of AGP-MMT on intestinal injury induced by ETEC infection than MMT treatment alone.

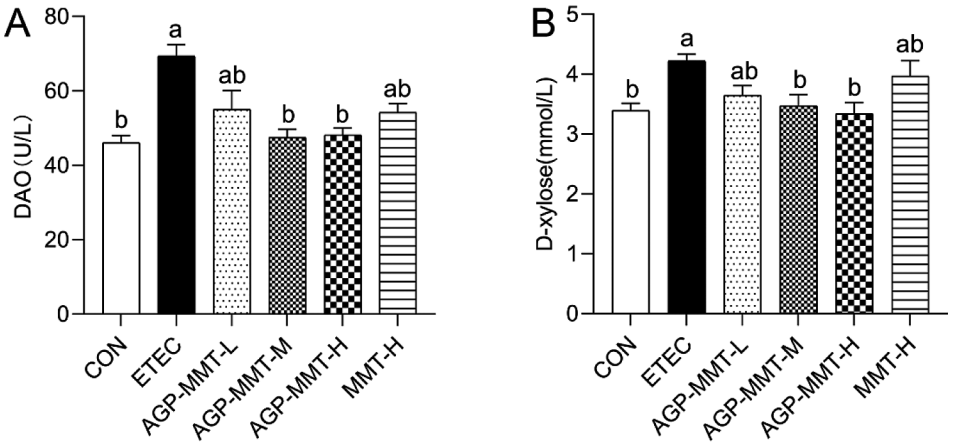

Fig. 4. Effect of different dose of AGP-MMT and MMT on intestinal permeability in ETEC challenged mice. Effect of different dose of AGP-MMT and MMT on (A) serum diamine oxidase (DAO) or (B) D-xylose in ETEC challenged mice. Data were expressed as means ± sem, n=8/group. Values within groups with different letters are significantly different ($p<0.05$).

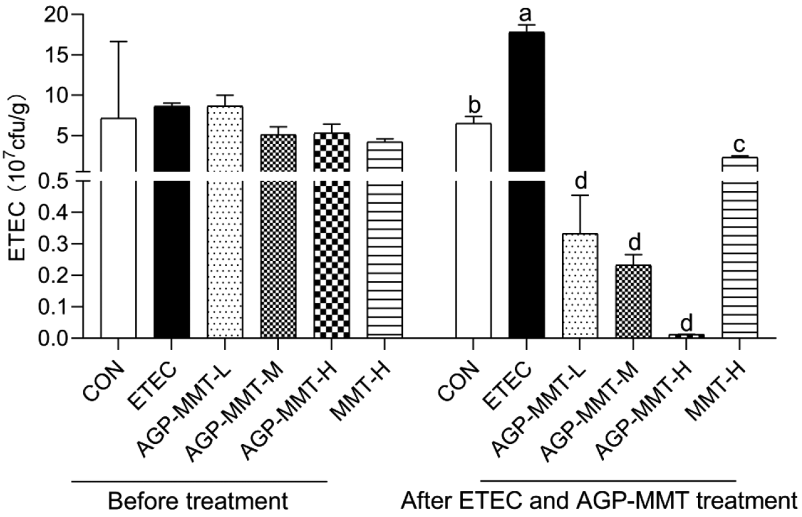

Fig. 5. Effect of AGP-MMT on the amount of fecal ETEC in ETEC challenged mice. Data were expressed as means ± sem, n=8/group. Values within groups with different letters are significantly different ($p<0.05$).

AGP-MMT maintained the gut barrier in mice with ETEC challenge

DAO and D-xylose are often regarded as important indexes of intestinal barrier injury (Yu et al. 2020). Mice treated with ETEC had increased ($p<0.05$) serum levels of DAO and D-xylose. Mice pretreated with AGP-MMT had decreased serum DAO and D-xylose, and reached a significant difference ($p<0.05$) both in the AGP-MMT-M and AGP-MMT-H group, compared with the ETEC group. In addition, there was no significant difference ($p>0.05$) of DAO and D-xylose between the AGP-MMT-H and MMT-H group (Fig. 4).

AGP-MMT alleviated ETEC shedding in stool of mice with ETEC challenge

Colonization of ETEC was defined by recovery of ETEC from the cultured mouse fecal bacteria (Rodea et al. 2017, Yan et al. 2017). There was no significant difference ($p>0.05$) in the concentration of ETEC in feces at the beginning of this study, implying a consistent ETEC loading between all groups (Fig. 5). Mice with ETEC infection had an increased ($p<0.05$) concentration of ETEC in feces at d 16 of the experiment, compared with the CON group. Mice pretreated with AGP-MMT had a decreased ($p<0.05$) fecal ETEC concentration compared with the ETEC group, though no significant difference was founded among AGP-MMT-L, AGP-MMT-M and AGP-MMT-H groups ($p>0.05$). More importantly, the concentration of fecal ETEC in the AGP-MMT-L, AGP-MMT-M and AGP-MMT-H groups was significantly lower ($p<0.05$) than the MMT-H group. These observations demonstrated that mice pretreatment with AGP-MMT alleviated ETEC shedding.

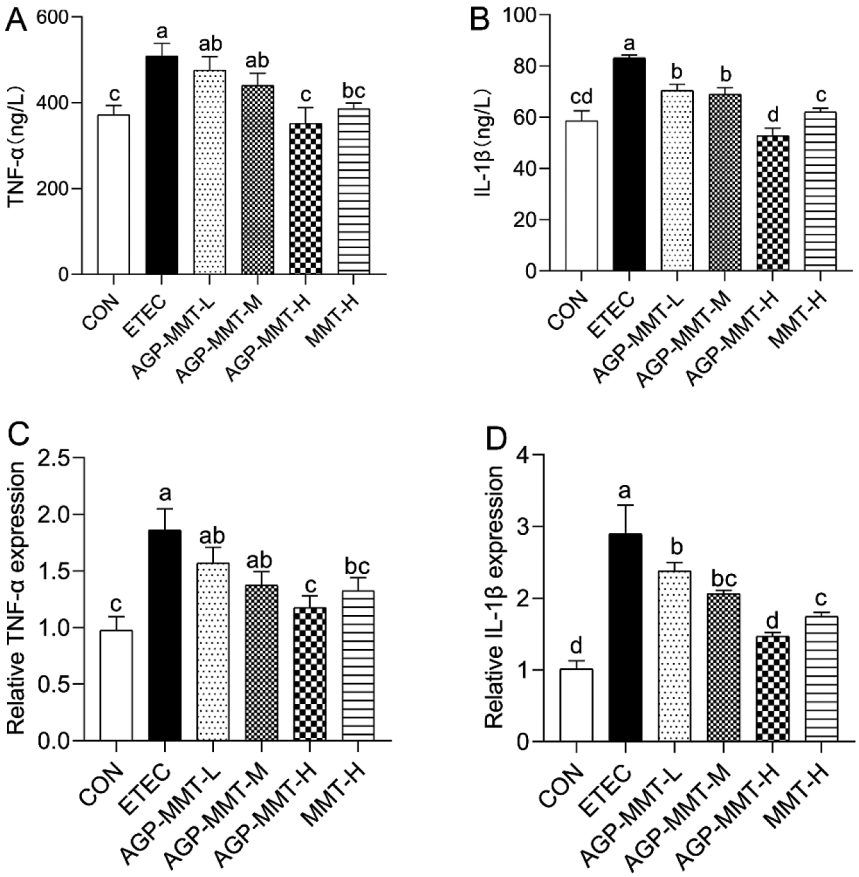

Fig. 6. Effect of different dose of AGP-MMT and MMT on inflammatory cytokines in ETEC challenged mice. Effect of different dose of AGP-MMT and MMT on (A) serum TNF-α, and (B) IL-1β in ETEC challenged mice. Effect of different dose of AGP-MMT and MMT on (C) the relative mRNA expression of TNF-α, and (D) IL-1β in the jejunum of mice with ETEC challenge. Data were expressed as means ± sem, n=8/group. Values within groups with different letters are significantly different ($p<0.05$).

AGP-MMT alleviated intestinal inflammation in mice with ETEC challenge

TNF-α and IL-1β are typical inflammatory cytokines in response to ETEC infection. In line with ETEC colonization results, ETEC challenge significantly increased serum levels of TNF-α and IL-1β (Fig. 6A-6B). AGP-MMT decreased the concentration of TNF-α and IL-1β in a dose dependent manner, and both inflammatory cytokines reached the lowest levels following treatment with high levels of AGP-MMT (AGP-MMT-H). In addition, IL-1β in the AGP-MMT-H group was lower ($p<0.05$) than in the MMT-H group, whereas no significant difference in TNF-α was found between the AGP-MMT-H group and MMT-H group.

The relative mRNA expression of TNF-α and IL-1β in the jejunum after AGP-MMT and MMT treatment showed a consistent result with serum TNF-α and IL-1β. ETEC infection significantly increased the relative mRNA expression of TNF-α, whereas AGP-MMT decreased the relative mRNA expression of TNF-α in a dose dependent manner (Fig. 6C). Moreover, the relative mRNA expression of TNF-α was significantly lower ($p<0.05$) in the CON and AGP-MMT-H group, compared with the ETEC group. AGP-MMT also significantly alleviated the up-regulated relative mRNA expression of IL-1β induced by ETEC infection, and AGP-MMT-H played a better remission role compared with the MMT-H group (Fig. 6D).

Discussion

MTT has been well known for its anti-diarrhea function, for example, Guarino et al. (2001) reported the protection role of MMT in the treatment of acute diarrhea though absorbing bacteria and toxin, and thus protecting the host intestinal barrier function (Guarino et al. 2001). However, the physicochemical properties of MMT, including absorption and ion exchange capacity, restrict its function in response to the intestinal barrier and inflammatory reaction. Brubaker et al. (2021) revealed the intestinal and systemic inflammation induced by symptomatic and asymptomatic ETEC infection (Brubaker et al. 2021). Based on the limitation of MMT, zinc-loaded, copper-loaded, and zinc/copper-loaded MMT have been developed and used in animal feed. For example, Jiao et al. (2017) reported

that copper/zinc-loaded MMT exhibited enhanced anti-microbial capacity against *Escherichia coli*, *Staphylococcus aureus*, and anti-fungal capacity against *Candida albicans* (Jiao et al. 2017). In contrast to zinc and copper, andrographolide exhibited a profound anti-inflammation function *in vitro* and *in vivo*. Su et al. (2020) reported that andrographolide at a dosage of 150 mg/kg per mouse alleviated intestinal inflammation and barrier function induced by lipopolysaccharide (Su et al. 2020). In this study, we successfully prepared AGP-MMT after sodium modification, polyethylene glycol modification of the raw MMT, and subsequent andrographolide loading. The microstructure of AGP-MMT showed spheroid particles, which was consistent with the structure of modified MMT with (3-Aminopropyl) triethoxysilane as previous described by Han et al. (2021) (Han et al. 2021). In addition, AGP-MMT showed lower interplanar spacing compared with the raw MMT, which was likely to be linked with the modification of MMT by sodium and polyethylene glycol, as Delbem et al. (2010) reported that sodium modification decreased the interplanar spacing of MMT (Delbem et al. 2010).

Most studies regarding the function of MMT focused on the anti-diarrhea function, including the duration of diarrhea, and the electrolyte balance of the intestine. For example, Guarino et al. (2001) reported the anti-diarrhea function of MMT in children (Guarino et al. 2001), Chang et al. (2007) reported the efficacy of dioctahedral smectite in treating patients with diarrhea (Chang et al. 2007). Limited studies involved the intestinal function, especially the intestinal barrier and inflammatory response. The intestine is composed of a physical and metabolic barrier against bacteria and endotoxin. Xia et al. (2019) have demonstrated that ETEC infection induced intestinal barrier injury *in vivo* and intestinal epithelial cell apoptosis (Xia et al. 2019). Another finding of this study was that AGP-MMT not only alleviated the loss of body weight, but also alleviated the gut injury induced by ETEC infection. In this study, AGP-MMT treatment reversed the reduction of body weight losses in ETEC challenged mice in a dose dependent manner, and attenuated the mucosal morphology change. In accordance with the intestinal morphology, AGP-MMT treatment also alleviated the reduction of villus height and the ratio of villus height/crypt depth, and restored the levels of serum DAO and D-xylose in ETEC challenged mice. Surprisingly, our results were in contrast with results in an ETEC challenged piglet model; Almeida et al. (2016) did not detect any effect of smectite on the intestinal morphology, body weight, villus height and the ratio of villus height/crypt in ETEC challenged piglets (Almeida et al. 2013). The main reason for the difference between these two studies may be associated with the dosage of MMT and animal difference. In addition, the andrographolide might be another reason responsible for the different results; Jiang et al. (2020) revealed that andrographolide reduced intestinal permeability in a dextran sulfate sodium induced mice colitis model (Jiang et al. 2020). Consistently, AGP-MMT played a better regulation role on the villus height and the ratio of villus height/crypt depth, and lower ETEC shedding in the stool compared with equal levels of MMT alone.

The protective role of AGP-MMT on the intestinal function was further verified by the intestinal inflammatory response. In the present study, AGP-MMT treatment significantly alleviated the inflammatory reaction, especially the intestinal inflammation, as indicated by the results that AGP-MMT reduced the typical inflammatory cytokines, especially TNF-α and IL-1β in the serum of ETEC challenged mice. Further analysis showed that the relative mRNA expression of TNF-α and IL-1β in the jejunum of ETEC challenged mice decreased after AGP-MMT treatment, and the protein and mRNA of IL-1β were significantly lower in AGP-MMT compared with the MMT group. The more potent anti-inflammation capacity in the AGP-MMT group than the MMT group was likely to be associated with andrographolide. Ren et al. (2019) revealed that endotoxin secreted from ETEC plays an important role in intestinal inflammation (Ren et al. 2019). In addition, Guo et al. (2014) found that andrographolide interferes with quorum sensing to reduce cell damage caused by avian pathogenic *Escherichia coli* (Guo et al. 2014). Consistently, the concentration of ETEC in feces was significantly lower in AGP-MMT compared with MMT. The observation in this study was consistent with the anti-inflammation role of andrographolide or its derivative in human ulcerative colitis and colitis mice models, as recently reported (Zhu et al. 2018, Kim et al. 2019, Jiang et al. 2020). However, further studies are needed to explore the accurate mechanism of AGP-MMT in mice with ETEC challenge.

Conclusions

AGP-MMT was established through loading of MMT with andrographolide, and AGP-MMT was more effective in alleviating intestinal barrier function injury and inflammation in mice with ETEC infection than MMT alone. This study provides a promising alternative to remedy ETEC infection.

Acknowledgements

This work was support by a grant from the National Key Research and Development Program of China (Grant No.2021YFD1300300), Key R&D and promotion projects in Henan Province (Grant No. 212102110161) and the Scientific Research Foundation for High-level talents in Henan Technology University (Grant No.31401373).

References

Ala'a A, Canatan H, and Ezeamuzie CI (**2009**) In vitro and in vivo anti-inflammatory effects of andrographolide. Int Immunopharmacol 9: 313-318.

Almeida JAS, Liu Y, Song M, Lee JJ, Gaskins HR, Maddox CW, Osuna O, Pettigrew JE (**2013**) Escherichia coli challenge and one type of smectite alter intestinal barrier of pigs. J Anim Sci Biotechnol 4: 52.

Brubaker J, Zhang X, Bourgeois AL, Harro C, Sack DA, Chakraborty S (**2021**) Intestinal and systemic inflammation induced by symptomatic and asymptomatic enterotoxigenic E. coli infection and impact on intestinal colonization and ETEC specific immune responses in an experimental human challenge model. Gut Microbes 13: 1891852.

Burgos RA, Alarcón P, Quiroga J, Manosalva C, Hancke J (**2021**) Andrographolide, an anti-inflammatory multitarget drug: all roads lead to cellular metabolism. Molecules 26: 5.

Bywater RJ (**2005**) Identification and surveillance of antimicrobial resistance dissemination in animal production. Poultry Sci 84: 644-648.

Chang FY, Lu CL, Chen CY, Luo JC (**2007**) Efficacy of dioctahedral smectite in treating patients of diarrhea-predominant irritable bowel syndrome. J Gastroen Hepatol 22: 2266-2272.

Chen J, Wan CM, Gong ST, Fang F, Sun M, Qian Y, Huang Y, Wang BX, Xu CD, Ye LY, Dong M, Jin Y, Huang ZH, Wu QB, Zhu CM, Fang YH, Zhu QR, Dong YS (**2018**) Chinese clinical practice guidelines for acute infectious diarrhea in children. World J Pediatr 14: 429-436.

Cheng G, Hao H, Xie S, Wang X, Dai M, Huang L, Yuan Z (**2014**) Antibiotic alternatives: the substitution of antibiotics in animal husbandry? Front microbiol 5: 217.

Delbem, MF, Valera TS, Valenzuela-Diaz FR, Demarquette N (**2010**) Modification of a brazilian smectite clay with different quaternary ammonium salts. Quim Nova 33: 309-315.

Gaastra W, Svennerholm AM (**1996**) Colonization factors of human enterotoxigenic Escherichia coli (ETEC). Trends Microbiol 4: 444-452.

Ghosh P, Mondal S, Bera T (**2016**) Preparation and characterization of andrographolide nanoparticles for visceral leishmaniasis chemotherapy: In vitro and in vivo evaluations. Int J Pharm Pharmac Sci 8: 102-107.

Guarino A, Ashkenazi S, Gendrel D, Vecchio AL, Shamir R, Szajewska H (**2014**) European Society for Pediatric Gastroenterology, Hepatology, and Nutrition/European Society for Pediatric Infectious Diseases Evidence-Based Guidelines for the Management of Acute Gastroenteritis in Children in Europe: Update 2014. J Pediatr Gastr Nutr 59: 132-152.

Guarino A, Bisceglia M, Castellucci G, Iacono G, Casali LG, Bruzzese E, Musetta A, Greco L (**2001**) Smectite in the treatment of acute diarrhea: a nationwide randomized controlled study of the italian society of pediatric gastroenterology and hepatology (SIGEP) in collaboration with primary care pediatricians. J Pediatr Gastroenterol Nutr 32: 71-75.

Guarino A, Vecchio AL, Pirozzi MR (**2009**) Clinical role of diosmectite in the management of diarrhea. Expert Opin Drug Metab Toxicol 5: 433-440.

Guo X, Zhang LY, Wu SC, Xia F, Fu YX, Wu YL, Leng CQ, Yi PF, Shen HQ, Wei XB, Fu BD (**2014**) Andrographolide interferes quorum sensing to reduce cell damage caused by avian pathogenic Escherichia coli. Vet Microbiol 174: 496-503.

Han C, Song J, Hu J, Fu H, Feng Y, Mu R, Xing Z, Wang Z, Wang L, Zhang J, Wang C, Dong L (**2021**) Smectite promotes probiotic biofilm formation in the gut for cancer immunotherapy. Cell Rep 34: 108706.

Hu C, Song J, You Z, Luan Z, Li W (**2012**) Zinc oxide-montmorillonite hybrid influences diarrhea, intestinal mucosal integrity, and digestive enzyme activity in weaned pigs. Biol Trace Elem Res 149: 190-196.

Jiang N, Wei Y, Cen Y, Shan L, Zhang Z, Yu P, Wang Y, Xu L (**2020**) Andrographolide derivative AL-1 reduces intestinal permeability in dextran sulfate sodium (DSS)-induced mice colitis model. Life Sci 241: 117164.

Jiao L, Lin F, Cao S, Wang C, Wu H, Shu M, Hu C (**2017**) Preparation, characterization, antimicrobial and cytotoxicity studies of copper/zinc- loaded montmorillonite. J Anim Sci Biotechno 8: 27.

Kim N, Lertnimitphun P, Jiang Y, Tan H, Zhou H, Lu Y, Xu H (**2019**) Andrographolide inhibits inflammatory responses in LPS-stimulated macrophages and murine acute colitis through activating AMPK. Biochem Pharmacol 170: 113646.

Liu H, Wang C, Gu X, Zhao J, Nie C, Zhang W, Ma X (**2020**) Dietary Montmorillonite Improves the Intestinal Mucosal Barrier and Optimizes the Intestinal Microbial Community of Weaned Piglets. Front Microbiol 11: 593056.

Ma T, Peng W, Liu Z, Gao T, Liu W, Zhou D, Yang K, Guo R, Duan Z, Liang W, Bei W, Yuan F, Tian Y (**2021**) Tea polyphenols inhibit the growth and virulence of ETEC K88. Microb Pathogenesis 152: 104640.

Massaro M, Colletti CG, Lazzara G, Riela S (**2018**) The Use of Some Clay Minerals as Natural Resources for Drug Carrier Applications. J Funct Biomater 9: 58.

Ren M, Cai S, Zhou T, Zhang S, Li S, Jin E, Che C, Zeng X, Zhang T, Qiao S (**2019**) Isoleucine attenuates infection induced by E. coli challenge through the modulation of intestinal endogenous antimicrobial peptide expression and the inhibition of the increase in plasma endotoxin and IL-6 in weaned pigs. Food Funct 10: 3535-3542.

Rodas C, Mamani R, Blanco J, Blanco JE, Wiklund G, Svennerholm AM, Sjöling A, Iniguez V (**2011**) Enterotoxins, colonization factors, serotypes and antimicrobial resistance of enterotoxigenic Escherichia coli (ETEC) strains isolated from hospitalized children with diarrhea in Bolivia. Braz J Infect Dis 15: 132-137.

Rodea GE, Montiel-Infante FX, Cruz-Córdova A, Saldaña--Ahuactzi Z, Ochoa SA, Espinosa-Mazariego K, Hernández-Castro R, Xicohtencatl-Cortes J (**2017**) Tracking bioluminescent ETEC during in vitro BALB/c mouse colonization. Front Cell Infect Microbiol 7: 187.

Sargeant HR, McDowall KJ, Miller HM, Shaw MA (**2010**) Dietary zinc oxide affects the expression of genes associated with inflammation: Transcriptome analysis in piglets challenged with ETEC K88. Vet Immunol Immunop 137: 120-129.

Su HM, Mo JL, Ni JD, Ke HH, Bao T, Xie JH, Xu Y, Xie LH, Chen W (**2020**) Andrographolide exerts antihyperglycemic effect through strengthening intestinal barrier function and increasing microbial composition of akkermansia muciniphila. Oxid Med and Cell Longev 2020: 6538930.

Vaseeharan B, Thaya R (**2014**) Medicinal plant derivatives as immunostimulants: an alternative to chemotherapeutics and antibiotics in aquaculture. Aquacult Int 22: 1079-1091.

Wang P, Chen Q, Gan L, Du X, Li Q, Qiao H, Zhao Y, Huang J, Wang J (**2022**) Marginal zinc deficiency aggravated intestinal barrier dysfunction and inflammation through ETEC virulence factors in a mouse model of diarrhea. Vet Sci 9: 507.

Wang P, Yuan P, Lin S, Zhong H, Zhang X, Zhuo Y, Li J, Che L, Feng B, Lin Y, Xu S, Wu D, Burrin DG, Fang ZF (**2022**) Maternal and fetal bile acid homeostasis regulated by sulfated progesterone metabolites through FXR signaling pathway in a pregnant sow model. Int J Mol Sci 23: 6496.

Wang Q, Zhan X, Wang B, Wang F, Zhou Y, Xu S, Li X, Tang L, Jin Q, Li W, Gong L, Fu A (**2022**) Modified montmorillonite improved growth performance of broilers by modulating intestinal microbiota and enhancing intestinal barriers, anti-inflammatory response, and antioxidative capacity. Antioxidants (Basel) 11: 1799.

Xia Y, Chen S, Zhao Y, Chen S, Huang R, Zhu G, Yin Y, Ren W, Deng J (**2019**) GABA attenuates ETEC-induced intestinal epithelial cell apoptosis involving GABA(A)R signaling and the AMPK-autophagy pathway. Food Funct 10: 7509-7522.

Yan F, Liu L, Cao H, Moore DJ, Washington MK, Wang B, Peek R, Acra SA, Polk DB (**2017**) Neonatal colonization of mice with LGG promotes intestinal development and decreases susceptibility to colitis in adulthood. Mucosal Immunol 10: 117-127.

Zhu Q, Zheng P, Chen X, Zhou F, He Q, Yang Y (**2018**) Andrographolide presents therapeutic effect on ulcerative colitis through the inhibition of IL-23/IL-17 axis. Am J Transl Res 10: 465-473.